Faculty Publications

3-21-2016

The closo-Si$_{12}$C$_{12}$ Molecule from Cluster to Crystal: A Theoretical Prediction

Xiaofeng F. Duan
Air Force Research Laboratory DoD Supercomputer Resource Center

Larry W. Burggraf
Air Force Institute of Technology

The closo-Si$_{12}$C$_{12}$ molecule from cluster to crystal: A theoretical prediction FREE

Xiaofeng F. Duan; Larry W. Burggraf

Check for updates

View Online   Export Citation   CrossMark

The Journal of Chemical Physics

Special Topic: Adhesion and Friction

Submit Today!

The closo-Si$_{12}$C$_{12}$ molecule from cluster to crystal: A theoretical prediction

Xiaofeng F. Duan[1,2,a)] and Larry W. Burggraf[2,a)]
[1]*Air Force Research Laboratory DoD Supercomputer Resource Center, Wright-Patterson Air Force Base, Ohio 45433, USA*
[2]*Air Force Institute of Technology, Wright-Patterson Air Force Base, Ohio 45433, USA*

The structure of closo-Si$_{12}$C$_{12}$ is unique among stable Si$_n$C$_m$ isomers (n, m > 4) because of its high symmetry, π–π stacking of C$_6$ rings and unsaturated silicon atoms at symmetrical peripheral positions. Dimerization potential surfaces reveal various dimerization reactions that form between two closo-Si$_{12}$C$_{12}$ molecules through Si–Si bonds at unsaturated Si atoms. As a result the closo-Si$_{12}$C$_{12}$ molecule is capable of polymerization to form stable 1D polymer chains, 2D crystal layers, and 3D crystals. 2D crystal structures formed by side-side polymerization satisfy eight Si valences on each monomer without large distortion of the monomer structure. 3D crystals are formed by stacking 2D structures in the Z direction, preserving registry of C$_6$ rings in monomer moiety. [http://dx.doi.org/10.1063/1.4943957]

I. INTRODUCTION

Charge transfer molecules serve in technologies of photovoltaics,[1] molecular electronics,[2] fluorescent chemosensors,[3] and molecular excitonics.[4] Here we report computer design of polymers and crystals from charge-transfer molecule closo-Si$_{12}$C$_{12}$ having properties that make them candidates for these technologies also. SiC materials technologies are expected to be much more robust at high temperatures than organometallic materials, expanding the temperature range of these technologies.

The structure of closo-Si$_{12}$C$_{12}$ is unique among stable Si$_n$C$_m$ isomers (n > 4) as regards its high symmetry, D$_{2h}$.[5,6] Closo-Si$_{12}$C$_{12}$ has a carbon region, two π-stacked C aromatic rings, capped by two opposite Si regions connected by Si–C bonds. Optical absorptions for closo-Si$_{12}$C$_{12}$ have large optical oscillator strengths distinguished by pure charge transfer between the silicon and carbon segregation regions.[6] Like ligand-metal charge-transfer organometallic molecules which support electron transfer between metal and ligand regions, closo-Si$_{12}$C$_{12}$ molecules exhibit charge transfer between carbon and silicon regions suggesting analogous opportunities for such molecules in photonics and excitonics. Absorptions involving charge transfer between the carbon and silicon regions produce lower excitation energies than for isomers having alternating Si–C bonding for which frontier orbital charge transfer is exclusively from separated carbon atoms to silicon atoms. The electron and the hole charge distribution patterns in excitations that we previously calculated for major photo-absorption transitions[6] show strong one-electron transition in the visible blue transfers charge from the silicon region to the carbon region, while a strong one-electron transition in the near infrared, at about half the energy of the blue transition, transfers charge from the carbon region to the silicon region.

Potential for closo-Si$_{12}$C$_{12}$ molecules may be even greater than the many other silicon carbon molecules which exhibit similar charge transfer properties because closo-Si$_{12}$C$_{12}$ molecules have the capability to self-assemble on graphitic surfaces forming arrays, as well as form 1D polymer chains, 2D polymer layers, and 3D crystals. Here we report optimization calculations using density functional theory (DFT) B3LYP/cc-pVTZ for three types of linkages between monomers to form polymers having parallel aromatic rings: (1) side-by-side monomers connected by 2 side Si–Si bonds, (2) staggered monomers connected by 2 Si–Si bonds, side and corner, (3) staggered monomers connected by 3 Si–Si bonds, one side to side and two corner-to-side bonds. We also use DFT to describe 2D and 3D crystals that can form. In a future report we will describe the optical properties of these systems that have potential as optical materials capable of exciton conduction.

II. METHODOLOGY

In previous work,[6,7] we identified the closo-Si$_{12}$C$_{12}$ cluster, optimized by DFT methods, as the most stable among numerous Si$_{12}$C$_{12}$ isomers at low temperature. We used the Combination of Stochastic Potential Surface Search and Pseudopotential Plane-Wave Car-Parinello Simulated Annealing Simulations (PSPW-CPMD-SA) to select low-energy candidate isomers. DFT methods were used to determine the energy order of the lowest energy isomers. In this study we report details of closo-Si$_{12}$C$_{12}$ molecular structure including singlet, triplet, and charged doublet states. Further, we investigate its interesting polymerization chemistry including dimerization of closo-Si$_{12}$C$_{12}$ in different configurations as well as possible structures for 2D and 3D crystals.

For the optimized geometry of the closo-Si$_{12}$C$_{12}$ cluster in ground S$_0$ state, we calculated the following: a natural orbital analysis[8] to obtain electron occupancy, orbital hybrids,

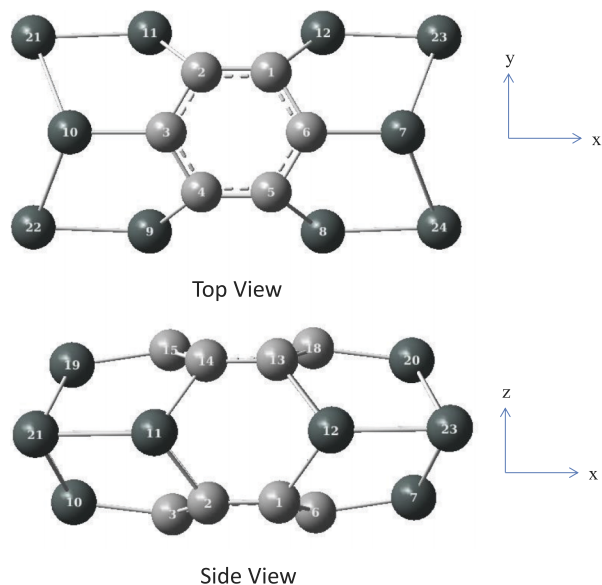a)Authors to whom correspondence should be addressed. Electronic addresses: xiaofeng.duan@wpafb.af.mil and larry.burggraf@us.af.mil.

FIG. 1. Closo-$Si_{12}C_{12}$ structure illustration with dark gray Si atoms and light gray C atoms.

CM5 atomic charges,[9] and Wiberg atomic valence index[10] as well as vibrational frequency to predict its infrared and Raman spectra. We optimized geometries for closo-$Si_{12}C_{12}$ in triplet T_0 state and anion doublet D_0 state to calculate their electronic properties and we performed vibrational frequency calculations to confirm the minimum energy states and to obtain the zero-point energies. We performed relaxed potential energy surface (PES) scans for constrained X, Y, and Z orientations to study the dimerization of the closo-$Si_{12}C_{12}$ cluster. For each dimer we optimized geometries simultaneously for monomers at each fixed inter-monomer distance moving in from both furthest distance as large as 15.0 Å and out from the nearest distance as small as 1.6 Å. In this way two PES segments were discovered. Geometries at the intersection provided starting structures for a TS search for dimerization by applying the Synchronous Transit-guided Quasi-Neuton (STQN) method.[11] The above calculations were done using DFT B3LYP hybrid functional[12] with cc-pVTZ basis sets.[13] Corroborating calculations for the transition state region were done using DFT PBE0 hybrid functional.[14] Periodic Boundary Condition (PBC) calculations were used

TABLE I. The geometry parameters of closo-$Si_{12}C_{12}$ monomer, label as displayed in Figure 1, calculated at B3LYP/cc-pVTZ level of theory.

Bond distance (Å)		Bond angle (°)	
C_1–C_2	1.398	C_1–C_2–C_3	120.08
C_2–C_3	1.411	C_1–C_2–Si_{11}	122.87
C_2–Si_{11}	1.915	C_3–C_2–Si_{11}	100.93
C_3–Si_{10}	1.954	C_2–C_3–C_4	116.89
S_{11}–Si_{21}	2.334	C_2–C_3–Si_{10}	118.44
Si_{10}–Si_{21}	2.448	C_2–Si_{11}–C_{14}	94.13
		C_2–Si_{11}–Si_{21}	121.83
		C_3–Si_{10}–Si_{21}	111.69
		Si_{21}–Si_{10}–Si_{22}	102.45
		Si_{11}–Si_{21}–Si_{10}	74.36
		Si_{10}–Si_{21}–Si_{19}	66.88

TABLE II. Occupancy of natural bond orbitals and hybrids; CM5 atomic charges and Wiberg atomic valence index for symmetry independent bonds and atoms calculated at B3LYP/cc-pVTZ level of theory. (Atom numbering is referred to Figure 1.)

NBO bond	Occupancy	Hybrid	Atom	CM5 charge	Wiberg valence
$\sigma(C_2$–$C_1)$	1.97	C_1: sp$^{1.60}$	C_2	−0.15	3.86
		C_2: sp$^{1.60}$	C_3	−0.12	3.83
$\pi(C_2$–$C_1)$	1.69	C_1: sp$^{99.99}$	Si_{10}	+0.12	3.41
		C_2: sp$^{99.99}$	Si_{11}	+0.25	3.25
$\sigma(C_2$–$C_3)$	1.96	C_2: sp$^{1.80}$	Si_{21}	−0.04	3.05
		C_3: sp$^{1.75}$			
$\sigma(C_2$–$Si_{11})$	1.90	C_2: sp$^{3.00}$			
		Si_{11}: sp$^{2.34}$			
$\sigma(C_3$–$Si_{10})$	1.89	C_3: sp$^{2.65}$			
		Si_{10}: sp$^{2.13}$			
$\sigma(S_{11}$–$Si_{21})$	1.86	Si_{11}: sp$^{1.61}$			
		Si_{21}: sp$^{10.99}$			
$\sigma(Si_{10}$–$Si_{21})$	1.70	Si_{10}: sp$^{2.10}$			
		Si_{21}: sp$^{13.38}$			
$\sigma(Si_{10}$–$Si_{19})$	1.45	Si_{10}: sp$^{15.02}$			
		Si_{19}: sp$^{15.02}$			

to optimize 1D, 2D, and 3D closo-$Si_{12}C_{12}$ polymer structures using Becke's functional[15] and LYP correlation correction (BLYP)[16] with cc-pVTZ basis sets instead of hybrid functional to better enable convergence of DFT calculations. The PBC geometry optimizations were carried out on the Γ-point only. All the calculations were carried out employing the Gaussian 09 computational chemistry package.[17] The IR and Raman absorption spectra were convoluted as a sum of pseudo-Voigt functions with a full-width-half-maximum value of 0.185 eV, using the software package SWizard.[18]
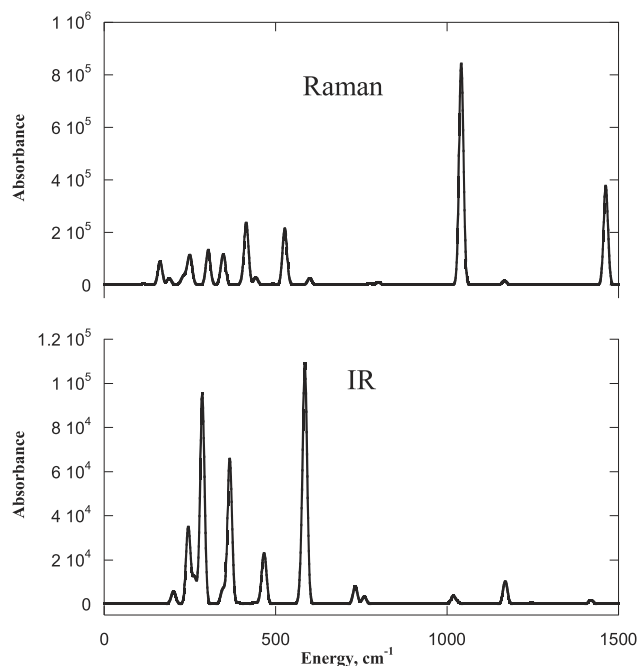

FIG. 2. Calculated IR and Raman spectra of closo-$Si_{12}C_{12}$ molecule.

III. RESULTS AND DISCUSSION

A. Monomer structure

The structure, stability, and optical properties of the closo-$Si_{12}C_{12}$ monomer displayed in Figure 1 have been described in a previous paper.[6] Detailed information about the geometry and electronic structure is recaptured and elaborated here. Calculated bond distances and bond angles for the monomer are displayed in Table I, referring to the structure shown in Figure 1. The closo-$Si_{12}C_{12}$ monomer structure is highly symmetrical, having D_{2h} point group symmetry. The structure contains two stacked C_6 aromatic rings that are connected to four Si atoms in two Si_4 caps at opposite ends of the molecule. There are three kinds of symmetrically distinct Si atoms: side Si atoms (8, 9, 11, 12),

corner Si atoms (21, 22, 23, 24), and end Si atoms (7, 10, 19, 20).

In Table I, the aromatic character of two C_6 rings is revealed by C–C distances of ~1.40 Å (compared to 1.42 Å in graphite and 1.40 Å in benzene) and C–C–C bond angles of $120°$–$122°$. The two C_6 rings are bridged by four side Si atoms (8, 9, 11, and 12) with C–Si distances of 1.92 Å. The close distance between the two C_6 rings is 2.80 Å which indicates a very strong π–π interaction as compared to weaker interactions between graphite planes separated by 3.35 Å.[19] A slightly folded Si_4 rhombus, which is the most stable structure of Si_4 isomers,[20] having edge Si–Si distances of 2.45 Å, caps the cluster at the both ends by attaching to four bridge Si atoms at Si–Si distance of 2.33 Å and four C (3, 6, 15, 18) atoms of two C_6 rings at Si–C distance of 1.95 Å. Bonding
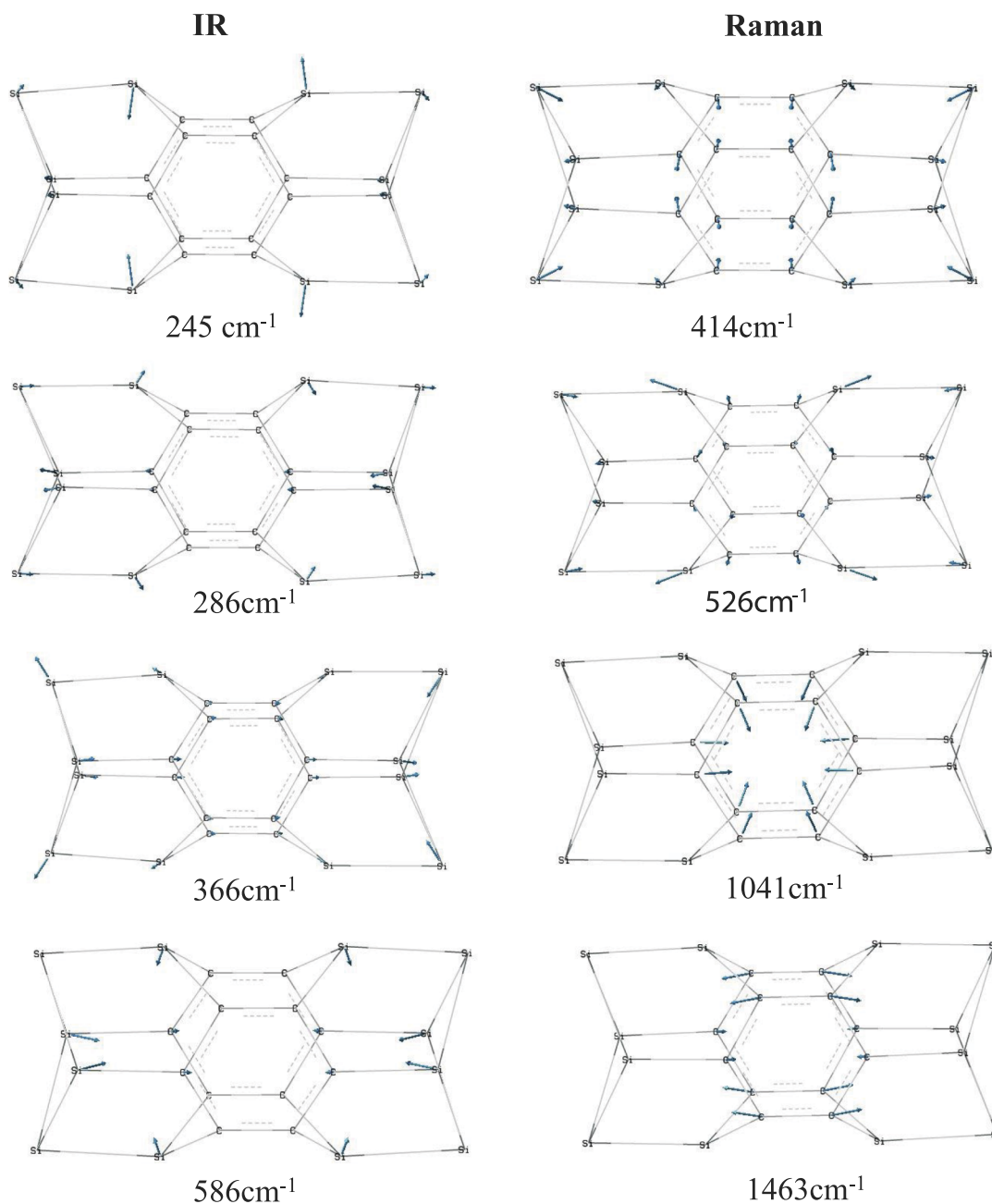

IR

245 cm⁻¹

286cm⁻¹

366cm⁻¹

586cm⁻¹

Raman

414cm⁻¹

526cm⁻¹

1041cm⁻¹

1463cm⁻¹

FIG. 3. Normal modes of IR and Raman spectral peaks for closo-$Si_{12}C_{12}$ molecule.

in the stacked C_6 aromatic rings and the capped Si_4 rhombus contributes to the superior thermodynamic stability of this structure relative to other $Si_{12}C_{12}$ isomers, consistent with the Si_nC_m bond stability index.[21]

The occupancy of natural bond orbitals and hybrids, the CM5 atomic charges as well as the Wiberg atomic valence indices for symmetry independent bonds and atoms are displayed in Table II. The Wiberg valence index separates the electron density into atomic and diatomic contributions interpreted as charges and bond orders, respectively. It illustrates that the valence of all C atoms is nearly saturated while the Si atoms have some free valence, especially the Si atoms at the four corners of the structure, analogous to silicon nanomaterials.[22] Because of the free valences on Si atoms, or dangling bonds, the polymerization of the cluster can occur readily.

The vibrational normal modes of the S_0 structure were calculated. The fact that no imaginary frequencies are found indicates the structure is in a minimum ground state. The IR and Raman spectra are plotted in Figure 2 and the normal modes corresponding to the major peaks of IR and Raman absorptions are shown in Figure 3. As seen in Figure 2, the majority of absorptions for both IR and Raman are in the 200–600 cm^{-1} energy range while two large Raman absorptions appear in the high energy range of 1000–1500 cm^{-1}. The normal mode analysis shown in Figure 3 illustrates that low energy absorptions mainly correspond to the motions of Si atoms and two high energy absorptions are predominantly caused by the stretching and breathing of C_6 rings. The similarity of vibrational frequencies of these two Raman modes to those of benzene rings (1586 cm^{-1} and 992 cm^{-1} respectively)[23] illustrates again that the aromatic character in the two C_6 rings is retained in the cluster.

To inspect the properties of the molecule for other stable electronic states, we performed geometry optimizations and calculated vibrational frequencies for the triplet state T_0 of the neutral molecule and the doublet state D_0 of the anion. The structural bonding parameters and energetic properties for these two states are listed in Table III. For convenience of comparison, the parameters and properties of singlet state are listed in the same table.

The original D_{2h} point group (PG) symmetry in S_0 state is no longer maintained in the structures of the T_0 and D_0 states. Instead, both T_0 and D_0 structures have C_{2v} symmetry with a C_2 axis in the Y direction. The vibrational frequencies calculations confirm that these two structures are energy minima. The T_0 state has an electronic total symmetry of $^3B_2$ with energy 0.45 eV higher than the S_0 state. Compared to the S_0 structure, the PG symmetry of the D_0 and T_0 structures is degraded from D_{2h} to C_{2v} mainly due to the shortening of C_4–C_5, C_2–Si_{11}, and C_3–Si_{10} and lengthening of Si_9–Si_{22} as well as their symmetry related partners. The presence of a dipole moment of 1.398 D with the vector along the Y direction (Figure 1 top view) indicates that the negative charge is distributed more toward the lower part of the asymmetric structure, toward the shortened C_4–C_5 bond. The D_0 state undergoes significant structure changes including bond length increase of C_4–Si_9 and Si_9–Si_{22} and decrease of C_3–Si_{10} bond, as well as symmetry related bonds. The dipole moment of 1.952 D with vector along Y direction also shows that the charges are largely distributed on the lower part of the structure for the D_0 state. Using total electronic energies and zero point energy corrections, from S_0 and D_0 states we calculated an electron affinity of −2.81 eV for the closo-$Si_{12}C_{12}$ cluster which is consistent with the reported theoretical vertical electron affinity of −2.87 eV for a $Si_{12}C_{12}$ isomer.[24]

B. Dimerization

In the ground state closo-$Si_{12}C_{12}$ cluster, Si atoms have unsaturated valence as large as 0.95 for corner Si atoms as

TABLE III. Structure, dipole moment, and energy comparisons for three electronic states for closo-$Si_{12}C_{12}$ monomer calculated at B3LYP/cc-pVTZ level of theory. (Atom numbering is referred to Figure 1.)

		Singlet S_0	Triplet T_0	Doublet D_0
Geometries	PG symmetry	D_{2h}	C_{2v}	C_{2v}
	C_1–C_2	1.398	1.392	1.399
	C_2–C_3	1.411	1.408	1.419
	C_3–C_4	1.411	1.418	1.417
	C_4–C_5	1.398	1.367	1.386
	C_2–Si_{11}	1.915	1.886	1.905
	C_3–Si_{10}	1.954	1.909	1.911
	C_4–Si_9	1.915	1.912	1.940
	Si_{11}–Si_{21}	2.334	2.329	2.349
	Si_9–Si_{22}	2.334	2.401	2.474
	Si_{10}–Si_{21}	2.448	2.452	2.449
	Si_{10}–Si_{22}	2.448	2.442	2.423
Dipole moment debye	Vector	(0.000 0.000 0.000)	(0.000 1.398 0.000)	(0.000 1.952 0.000)
Energy	Electronic state	^1A_g	$^3B_2$	$^2B_2$
	Total, a.u.	−3931.341 013	−3931.324 366	−3931.444 317
	Relative, eV	0.000	0.453	−2.811
	ZPE, eV	2.330	2.333	2.335
	EA, eV	−2.808		

shown by Wiberg valences in Table II. Therefore it is expected that various dimerization reactions between two closo-$Si_{12}C_{12}$ clusters can happen through the Si atoms. The small Wiberg index of four corner and four side silicon atoms particularly qualifies them as valence deficient having reactive dangling Si bonds. CM5 charges suggest that corner-side affinity will be larger than corner-corner affinity. Side-side dimers involve charge redistribution through conjugated C_6 rings, which is not possible for more electronically isolated corner Si atoms.

To describe dimerization reactions, we performed two kinds of relaxed PES scans by constraining the dimerization reaction coordinate in X, Y, or Z directions as shown in Figure 4. For each constrained direction PES scan, we obtained two segments of a potential surface (PES-I and PES-II) representing geometries for two different portions of a reaction coordinate through the process of dimerization. The two kinds of constrained PES scans are (i) PES-I, two monomers are moved toward each other in a specific orientation and (ii) PES-II, two monomers are separated from a stable dimer structure. Both PES segments are constrained to have equal Si–Si′ or C–C′ separation R as shown in Figure 5. The constrained dimer structures optimized on each PES segment are path dependent. For each direction (X, Y, and Z), we created a PES-I segment by placing the two monomers at a large distance (>6 Å) and then optimizing the geometry at each point while pushing them together at selected separations. For all the three directions we found that the PES-I represents mainly the van der Waals (VDW) interactions of two rigid monomers, i.e., the monomer structures are nearly unchanged. For the PES-II segments, we used the opposite process, after first forcing the two monomers near enough to react to form a dimer, we then pulled them apart increasing R point by point. PSE-II scans involve bond forming and breaking between two monomers. On PES-IIs, at separations large enough to break the connecting bonds between two monomers, the structural features for the two monomers are still similar to those in their stable dimer structures. For all the three directions, minimum-energy wells were found on the PES-IIs. These dimer structures, with key bond length parameters listed, are shown in Figure 5. Their dimerization energies, E_{dim}, relative to the non-interacting monomers are listed in Table IV. For comparison, the pre-dimer structures on PES-I are also illustrated in Figure 5.

PES-I and PES-II cross each other at certain equal separations along the selected coordinate. The location (R_c) and energies (E_c) of cross points of the two PESs are also listed in Table IV. The crossing point must be at an equal or higher energy than a transition state connecting the separated monomers and the dimer. At the crossing points, the structures on PES-I and PES-II are distinguishable from each other, indicating the minimum-energy transition from monomers to dimers does not simply occur at the crossing point. A reaction coordinate including the minimum-energy transition states (TS) involves more bond breaking than on PES-I. The nearly zero cross point energies as well as the curve slopes of PES-I and PES-II suggest there may be no TS for formation of Y or Z dimers from monomers. To corroborate these results, we repeated the constrained direction scans for the PES sections near the crossing points using the PBE0 functional. We obtained qualitatively similar results to those using the B3LYP functional.

The inter-monomer distance in the X direction R_X corresponds to the distance between two Si atoms at the end of each monomer as shown in Pre-Dimer-X in Figure 5. As R_X decreases, the PES-I increases monotonically and becomes steep when R_X is ~3.5 Å. A minimum energy structure, labeled as Dimer-X in Figure 5, was found on the PES-II when R_X is equal to 2.4 Å. PES-II climbs sharply from the energy minimum as R_X is increased. As revealed by the bond distances shown in Figure 5(a), Dimer-X is formed by two Si–Si′ bonds connecting corner Si atoms in the monomers. The monomers are significantly deformed in the dimer so that the PG symmetry of the minimum energy structure is degraded to Cs symmetry from the original D_{2h} on PES-I. As shown in Table IV, the dimerization energy of Dimer-X is as small as −0.09 eV. The two PESs cross at $R_X = 2.80$ Å. Beginning from PES-I and PES-II crossing point structures, the STQN method[11] was used to find a TS structure having one imaginary frequency that connects the dimer and pre-dimer. It is labeled as Dimer-X-TS, illustrated in Figure 5(a). In the TS geometry for both B3LYP and PBE0 functionals, two Si–Si′
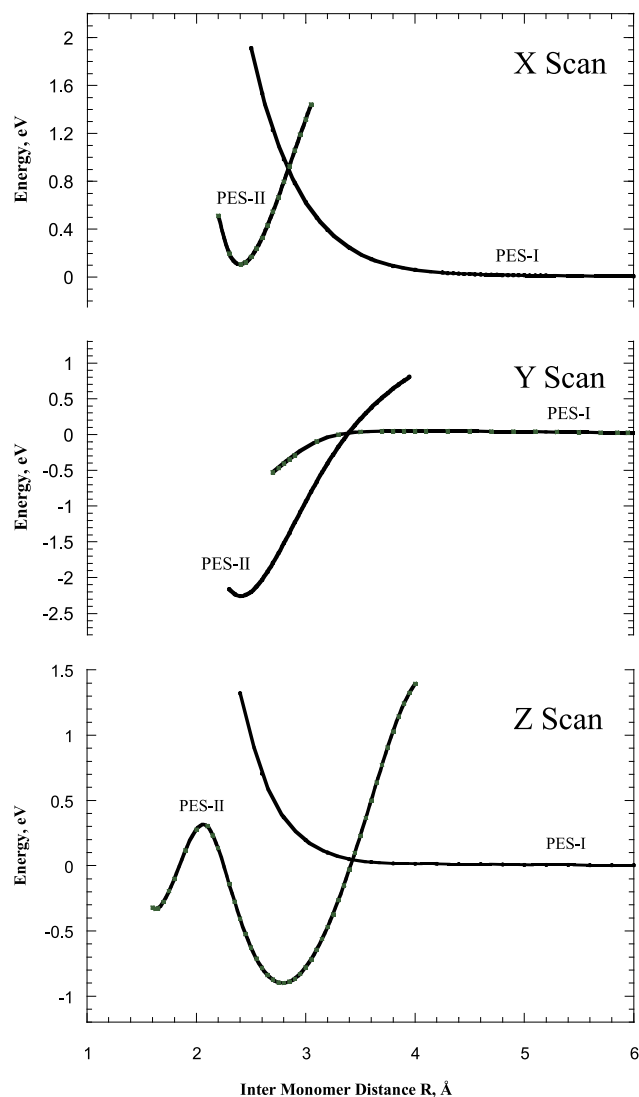

FIG. 4. Relaxed potential energy surface (PES) scans for two closo monomers approaching each other in X, Y, and Z directions.
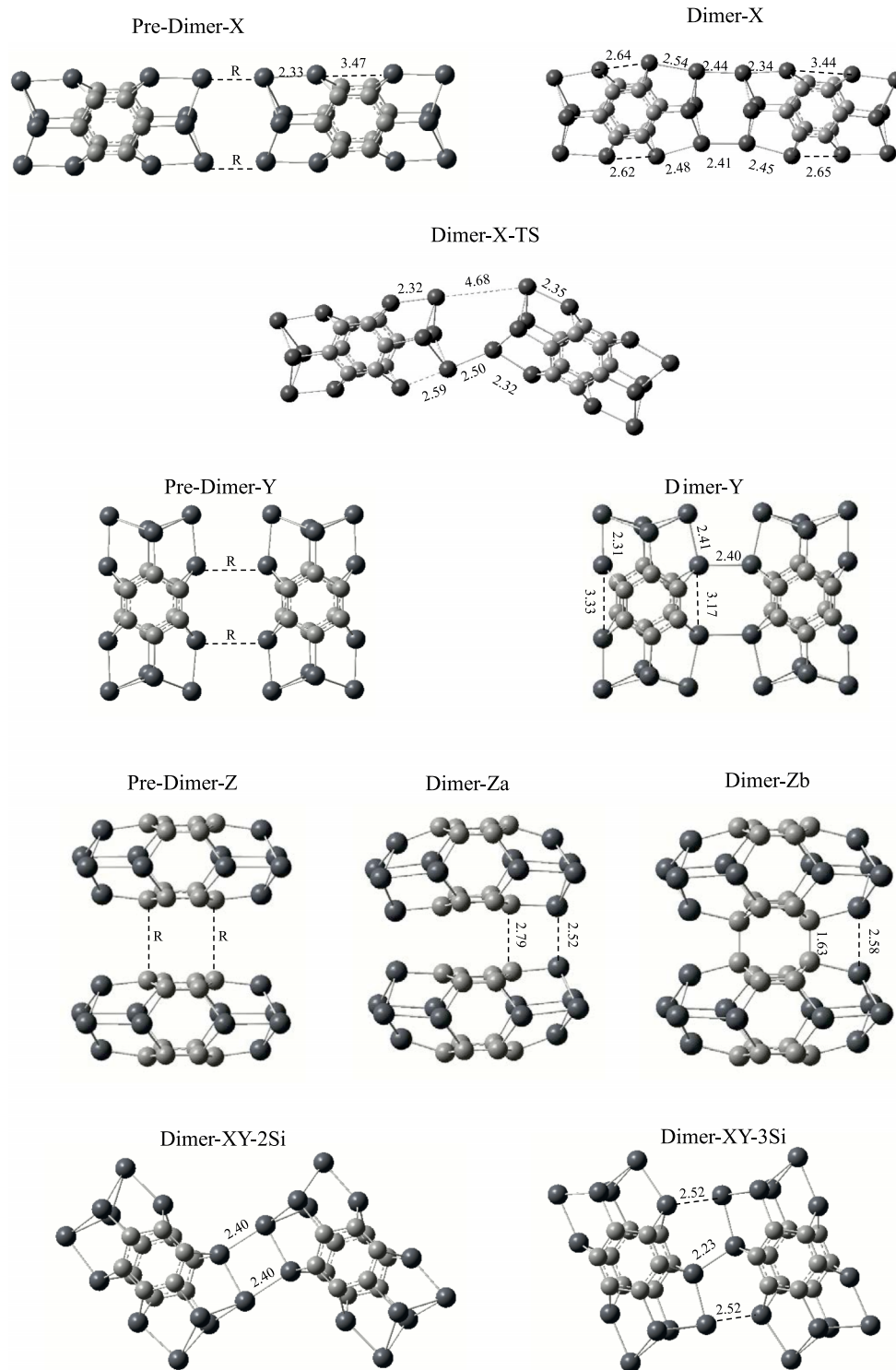
FIG. 5. (a) Pre-dimer illustration, dimer structures along X, Y, and Z directions, as well as the transition state structure along X direction optimized at B3LYP/cc-pVT level of theory. The key bond distances showing formation of dimer bonds are displayed. (b) Dimer structures along XY direction optimized at B3LYP/cc-pVT level of theory. The key bond distances showing formation of dimer bonds are displayed.

TABLE IV. Dimerization energies E_{dim}, PES cross point location R_c, and energy E_c calculated at B3LYP/cc-pVTZ level of theory.

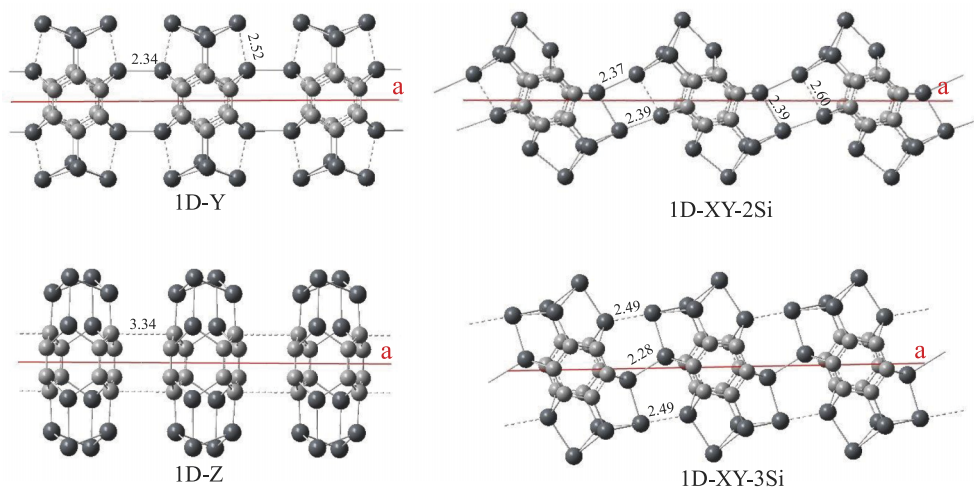|	(Monomer)$_2$	Dimer-X	Dimer-X-TS	Dimer-Y	Dimer-Za	Dimer-Zb	Dimer-XY-2Si	Dimer-XY-3Si
E_{dim}, eV	0.00	−0.088	+0.511	−2.258	−0.900	−0.331	−1.486	−2.513
R_c, Å		2.840		3.940	3.426			
E_c, eV		0.903		0.049	0.046			

FIG. 6. Optimized 1D polymer structures.

bonds are formed unsymmetrically; constraining these to be symmetrical yields a higher energy because of less favorable orientation of the lone pairs. The lone pair sp^3 hybridization is oriented at an open angle relative to the Si–Si separation vector in symmetrical PES scan for X-direction dimerization. The TS structure shows the dimerization process is stepwise by first forming an inter monomer Si–Si′ bond. The TS has calculated an activation energy of 0.51 eV with B3LYP functional and 0.32 eV with PBE0 functional. Our analysis of the PSE-I and PSE-II curves suggests that the relatively large activation energy and difficulty of dimerization in X direction can be attributed to the large deformation of sp^3 hybridization due to steric constraints for two corner Si atoms in the dimerization process.

For the Y direction, dimerization the inter monomer distance R_Y is taken as the distance between two Si atoms at the side of the two monomers as shown in Pre-Dimer-Y in Figure 5(a). The PES-I rises slowly as R_Y becomes shorter with the highest energy of ~0.05 eV when R_Y reaches approximately 3.94 Å and then slopes downward. PES-II rises sharply in the opposite direction following formation of a stable dimer at R_Y = 2.40 Å with a relative energy of −2.26 eV, labeled as Dimer-Y in Figure 4. Although there is a small energy barrier of 0.05 eV on PES-I, which is mostly the energy barrier for VDW interaction of two isolated monomers, the energy at the cross point (R_Y = 3.40 Å) of two PESs is nearly zero. Two inter-monomer Si–Si′ bonds are formed in the dimer and the geometric features of the monomer are mostly maintained. The stability of Dimer-Y and the steepness of PES-II as well as the flatness of PES-I warrant that a large exothermic dimerization reaction readily takes place without activation energy in the Y direction.

In the Z direction, the inter-monomer distance R_Z is the distance between two C atoms in each monomer as shown in

TABLE V. Lattice parameters, symmetries, and polymerization energies E_{pol} calculated at BLYP/cc-pVTZ level of theory.

1D polymerization		1D-Y	1D-XY-2Si	1D-XY-3Si	1D-Z
	E_{pol}, eV	−1.399	−1.083	−2.824	−0.332
	a, Å	6.748	8.842	7.233	6.542
2D polymerization		2D-Y	2D-XY-2Si	2D-XY-3Si	
	E_{pol}, eV	−2.389	−2.953	−4.422	
	a, Å	7.507	8.695	7.218	
	b, Å	10.199	8.695	10.669	
	γ, °	90.00	84.50	85.70	
	Lattice symmetry	Rectangular p2 mm	Oblique p2	Oblique p2	
3D polymerization		3D-Y	3D-XY-2Si	3D-XY-3Si	
	E_{pol}, eV	−2.790	−4.505	−5.652	
	a, Å	7.309	8.668	7.137	
	b, Å	10.100	8.668	10.562	
	c, Å	5.743	6.313	6.021	
	α, °	90.00	90.00	90.00	
	β, °	90.00	90.00	90.00	
	γ, °	90.00	86.66	86.57	
	Lattice symmetry	Monoclinic pmmm	Monoclinic p112/m	Triclinic p112/m	

Pre-Dimer-Z in Figure 5. PES-I energy increases slightly as the two monomers get closer and then it rises sharply after R_Z reaches 3.3 Å. PES-I crosses PES-II at R_Z = 3.4 Å with a small energy of 0.05 eV. Due to this non-zero crossing point energy, a small activation energy for dimerization in Z direction could be possible. However, application of STQN method that was productive for TS of X dimerization with geometries at crossing point of Z PES-I and PES-II was unproductive to locate a TS, suggesting that there is no transition state energy for Z dimerization.

On PES-II in the Z direction, we located two dimer isomers. The first dimer, labeled as Dimer-Za in Figure 5(a), has a relative energy of −0.90 eV. This dimer is stabilized because of a strong π-stacking interaction between the C_6 rings of the two monomers and additionally two weak Si–Si' bonds with a bond length of 2.52 Å. The monomer moieties in the dimer are bent relative to each other to favor π-stacking and Si–Si' bonding. If the two monomer subunits are pushed together further over a large energy barrier of

1.20 eV at R_Z = 2.1 Å, the second dimer is formed when R_Z reaches 1.63 Å, shown in Figure 5(a) as Dimer-Zb. With a dimerization energy of −0.33 eV, Dimer-Zb has two weak C–C' bonds, two weak Si–Si' with bond lengths of 1.63 Å and 2.58 Å, respectively. The rather smaller stability of Dimer-Zb compared to Dimer-Za can be explained by the change of hybridization of C atoms from sp^2 to sp^3 to form the C–C bonds so that the aromatic character of C_6 ring in each monomer moiety vanishes.

Based on the ease of dimerization in Y direction and structural feature of four available side Si atoms on each monomer, two additional dimers labeled Dimer-XY-2Si and Dimer-XY-3Si in Figure 5(b) were optimized by off-stacking the monomer subunit of Dimer-Y relative to each other in X direction. Dimer-XY-2Si, obtained by sliding two Si atom positions, is formed by connecting monomers with two Si–Si' bonds of 2.39 Å length. Its dimerization energy is −1.49 eV. By moving up/down 1 Si position from Dimer-Y in X direction, Dimer-XY-3Si was optimized. Since there are 3
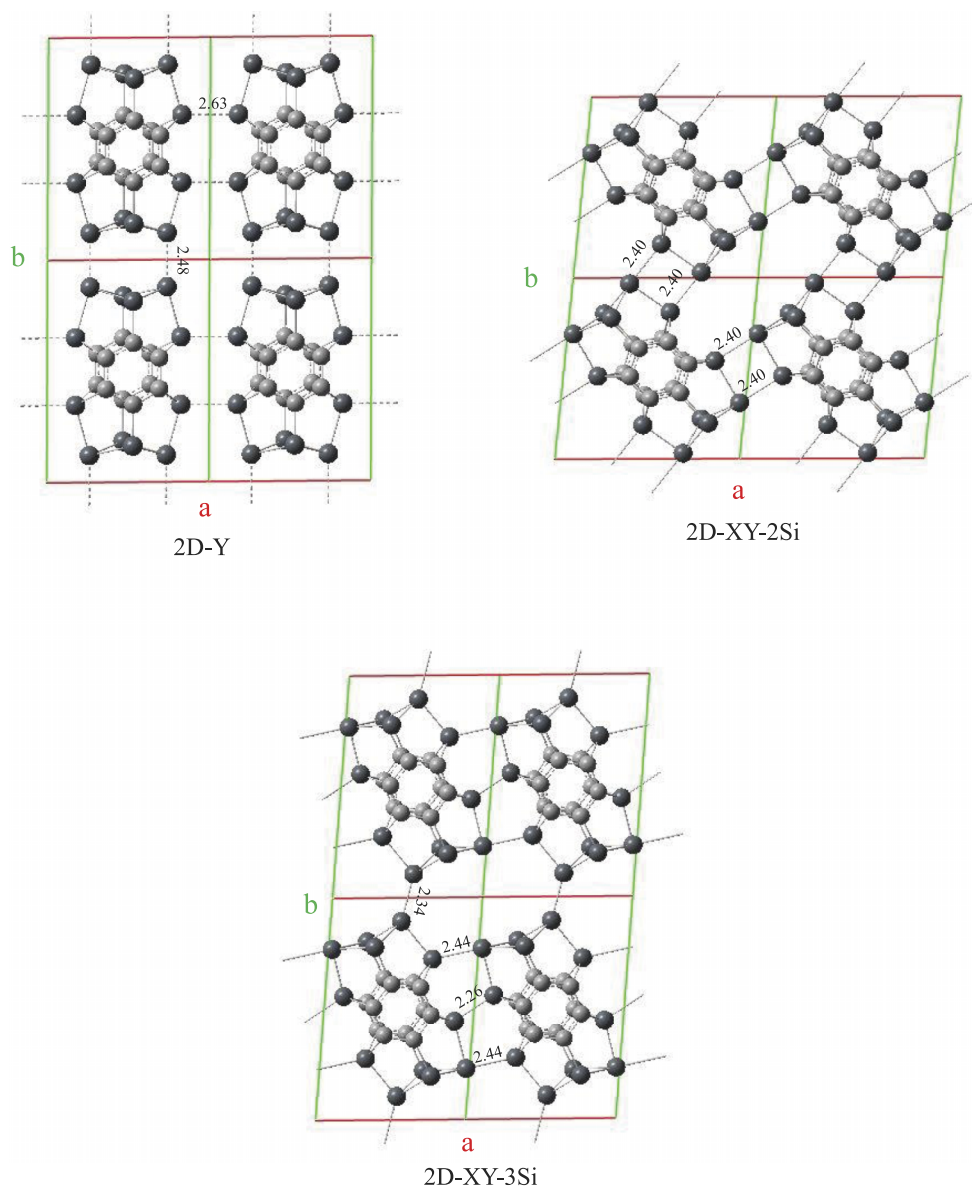

FIG. 7. Optimized 2D crystal structures.

Si–Si′ bonds connecting two monomer subunits, a stronger one in the center and two weaker ones on either side, among all the dimers Dimer-XY-3Si has the largest dimerization energy of −2.51 eV.

C. Polymerization

From analysis of Sec. III B about dimerization of closo-$Si_{12}C_{12}$ cluster in different directions, it can be predicted that polymerization in Z, Y, and XY directions is favored

by low activation energy and large stabilization energies. 1D polymerization in X direction is improbable due to the large reaction energy barrier and instability of the product. To investigate the mechanisms of the polymerization of closo-$Si_{12}C_{12}$, we carried out DFT solid state calculations with BLYP functional to optimize the 1D, 2D, and 3D crystal structures focused on Y, XY, and Z directions. Figure 6 shows the optimized 1D polymer structures analogous to dimerizations that form without significant activation energy. The lattice parameters, symmetries, and polymerization energies are
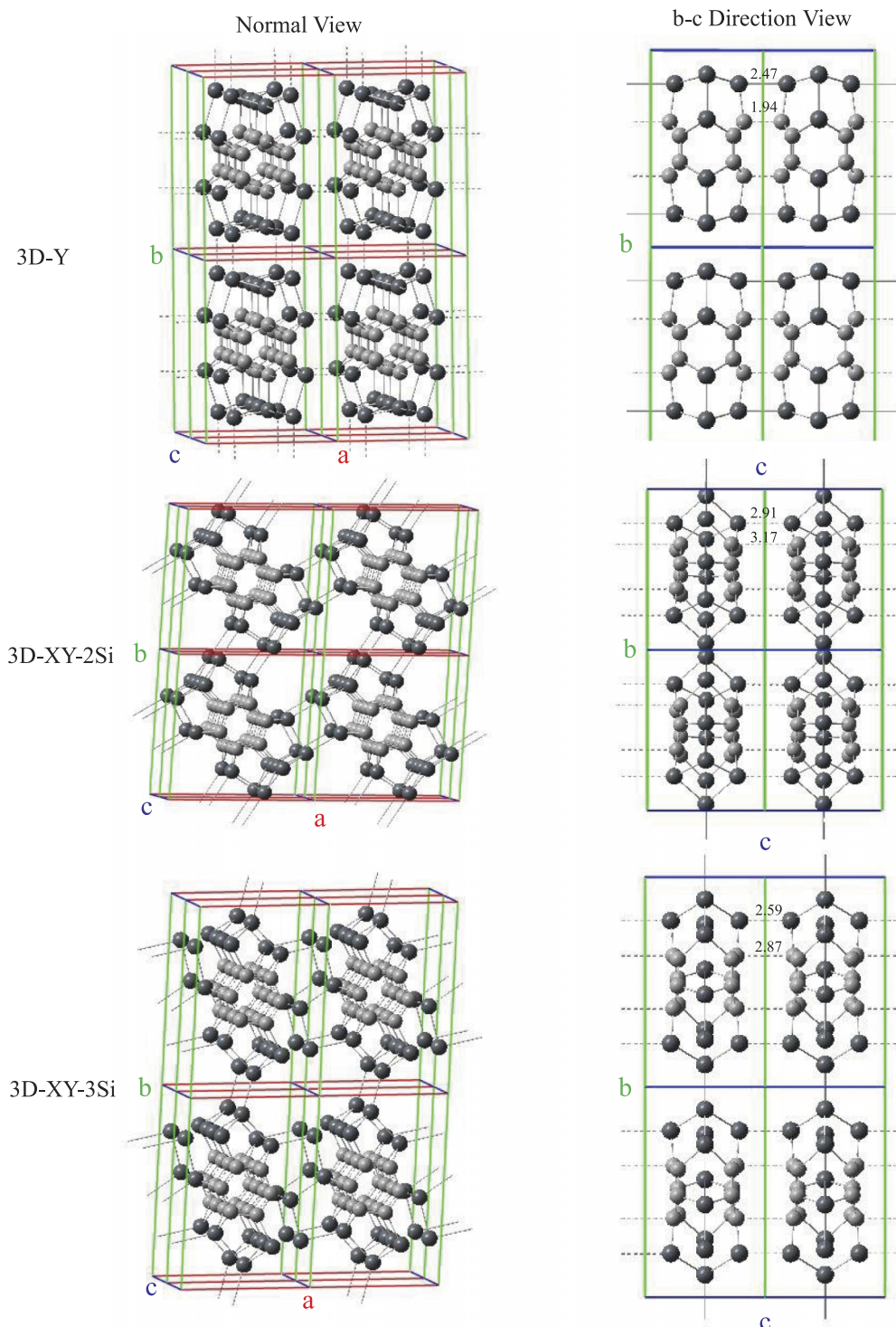

FIG. 8. Optimized 3D crystal structures in two lattice views.

listed in Table V. The polymer in Y direction, labeled 1D-Y, is formed by linking monomers by two Si–Si' bonds similar to Dimer-Y. The length of Si–Si' bonds 2.34 Å is slightly shorter than that in Dimer-Y and the polymerization energy, −1.399 eV, is much lower than the corresponding dimerization energy. Unlike Dimer-Za in which the monomer moieties are deformed to have strong C_6 ring π-stacking and a weak Si–Si' bonding, for the 1D polymer in Z direction labeled as 1D-Z in Figure 6, the polymerization interaction is mostly due to π-stacking interactions shown by the distance of 3.34 Å between C_6 rings yielding a smaller polymerization energy of −0.332 eV compared to the dimerization energy of Dimer-Z.

Analogous to two dimerizations in XY direction, two polymers were optimized, 1D-XY-2Si and 1D-XY-3Si as labeled in Figure 6. Although the 1D-XY-2Si polymerization energy of −1.083 eV is smaller than the corresponding dimerization energy of Dimer-XY-2Si, it is polymerized by connecting monomers with 2 Si–Si' bonds, 2.37 Å and 2.39 Å, respectively. For the case of polymer 1D-XY-3Si, it is formed by 3 Si–Si' bonds as in Dimer-XY-3Si, and has the largest polymerization energy of −2.824 eV among all the 1D polymers reported here.

By extending the 1D-Y and 1D-XY polymers in lattice *b* direction, we optimized three 2D polymers, named and displayed in Figure 7 as 2D-Y, 2D-XY-2Si, and 2D-XY-3Si. Their lattice parameters, symmetries, and polymerization energies are listed in Table V also. For 2D-Y, the 1D chains are connected to each other through two Si–Si' bonds in the X direction. Compared to Dimer-X, these Si–Si' bonds are about 0.1 Å longer. The Si–Si' bonds in Y direction, compared to 1D-Y, are lengthened by 0.3 Å. The polymerization from 1D-Y to 2D-Y is spontaneous, lowering the energy by 1.00 eV making the polymerization energy to be −2.39 eV. The polymer of 2D-XY-2Si can be formed readily when the unsaturated Si atoms on the moieties of one 1D-XY-2Si chain form two more Si–Si' bonds with those of another 1D-XY-2Si chain. The four Si–Si' bond lengths are equally 2.40 Å. The polymerization energy is greatly increased to −2.95 eV, more stable by 1.87 eV going from 1D-XY-2Si to 2D-XY-2Si. Similarly the one unsaturated Si atom on 1D-XY-3Si polymer can easily bond to its counterpart of another 1D chain to form 2D-XY-3Si polymer. The cross chain Si–Si' bond is 2.34 Å and this cross chain linkage contributes −1.60 eV to polymerization energy of 2D-XY-3Si to give −4.42 eV. It is predicted that 1D to 2D polymerization enhances polymerization energy for the three 2D polymers. The polymerization energy order of stability is changed from 1D-XY-3Si > 1D-Y > 1D-XY-2Si for 1D polymerization to 2D-XY-3Si > 2D-XY-2Si > 2D-Y for 2D polymerization.

The 3D polymers are formed by stacking 2D polymers in the Z direction. The three 3D polymers, labeled as 3D-Y, 3D-XY-2Si, and 3D-XY-3Si are shown in Figure 8. Their lattice parameters, symmetries, and polymerization energies are listed in Table IV also. For 3D-Y polymer, the 2D layers are bonded together in the Z direction with a bond pattern similar to Dimer-Zb, i.e., a weak C–C' (1.94 Å) bond, a Si–Si' (2.47 Å), and so enhances the polymerization energy by −0.40 eV to −2.79 eV, which is comparable to the dimerization energy of Dimer-Zb. The inter layer interaction in 3D-XY-2Si is

largely π-stacking as shown by the 3.37 Å of C–C' bond and 2.91 Å Si–Si' bond. The energy of π-stacking is as large as −1.50 eV and makes the polymerization energy of 3D-XY-2Si to be −4.51 eV. Interestingly the interlayer interaction in 3D-XY-3Si is intermediate between 3D-Y and 3D-XY-2Si. The C–C' bond of 2.87 Å indicates a stronger π–π interaction and the Si–Si' bond of 2.59 Å shows a weak bond between layers. The synergic interlayer interaction energy of −1.23 eV causes the polymerization energy of 3D-XY-3Si to be −5.65 eV. The transformation from 2D to 3D results in small structural changes of the 2D layers in all the situations and the order of polymerization energy is not changed either.

IV. CONCLUSIONS

Analysis of the closo-$Si_{12}C_{12}$ ground state structure indicates that strong π-stacked C_6 aromatic rings and the two capped Si_4 rhombi contribute to the superior thermodynamic stability of this structure relative to other $Si_{12}C_{12}$ isomers. Calculations of ground state properties of the closo isomer show that the valence of carbon atoms is mostly saturated while the Si atoms have incomplete valences, especially peripheral four corner Si atoms and four side Si atoms. Polymerization of these clusters can occur readily through the free valence on corner and side Si atoms. Calculated IR and Raman spectra and normal mode analysis show low absorption energy mainly corresponding to the motions of Si atoms and two high energy absorptions predominantly caused by the stretching and breathing of C_6 rings. This supports the conclusion that aromatic character in C_6 ring bonding is retained. Closo-$Si_{12}C_{12}$ molecular structures were also optimized for the electronic triplet and charged doublet states. Structural changes in these two states cause the D_{2h} symmetry of the singlet state to be degraded to C_{2v} with corresponding additional dipole moment formed in the Y direction (Figure 1).

Direction constrained PES scans for dimerization in X, Y, and Z directions reveal two segments of a potential surface (PES-I and PES-II) representing geometries on a reaction coordinate through the dimerization process. Analysis of crossing points of PES-I and PES-II permitted energy barriers and TS structures for dimerization to be deduced. Dimerization in the X direction is improbable at moderate temperatures for the endothermic reaction due to large energy barrier and entropy requirement for the complicated simultaneous bond changing mechanism inferred from the TS structure. Rapid exothermic dimerization reaction may take place in the Y and Z directions because of their negligible activation energies. In addition to the dimerization in X, Y, and Z directions, two staggered dimers were studied. Of all dimer possibilities, the staggered XY-3Si which forms three bonds is most stable. The Dimer-Y formed by two side-side bonds is slightly less stable while the staggered XY-2Si formed by two end-side Si–Si bonds is much less stable. Based on dimerization results, polymerization in Y and XY directions is favored by low activation energy and large stabilization energies while polymerization in the Z direction is disfavored. Four different 1D polymers extending dimer bonding are formed with stability order: 1D-XY-3Si > 1D-Y > 1D-XY-2Si > 1D-Z, shown in Figure 6.

The 2D crystal structures formed by side-side polymerization satisfy all eight Si valences on each monomer without large distortion of the monomer structure. In 2D-Y and 2D-XY-2Si structures adjacent monomers are connected by two Si–Si bonds, whereas in the 2D crystal 2D-XY-3Si adjacent monomers are connected by three Si–Si bonds. While dimerization in the X direction does not readily occur, corner-corner Si–Si' bonds do form in polymer chains in the 2D crystals 2D-Y and 2D-XY-3Si.

3D polymers are formed by stacking 2D structures in the Z direction, preserving registry of C_6 rings. In the most stable 3D structure, 3D-XY-2Si, stabilization by π-stacking is shown by the interlayer C–C distance 3.37 Å, weaker than the strong δ–δ interaction between C_6 rings in the monomer C_6 rings at 2.80 Å and comparable to the π–π stacking separation in graphite at 3.35 Å.

ACKNOWLEDGMENTS

[1]J. Roncali, P. Leriche, and P. Blanchard, Adv. Mater. **26**, 3821 (2014).

[2]E. Lörtscher, Nat. Nanotechnol. **8**, 381 (2013).

[3]J. Wu, W. Liu, J. Ge, H. Zhang, and P. Wang, Chem. Soc. Rev. **40**, 3483 (2011).

[4]S. K. Saikin, A. Eisfeld, S. Valleau, and A. Aspuru-Guzik, Nanophotonics **2**, 21 (2013).

[5]X. Wang, B. Wang, G. Chen, and J. Zhao, Chem. Phys. **355**, 31 (2009).

[6]X. F. Duan and L. W. Burggraf, J. Chem. Phys. **142**, 034303 (2015).

[7]X. F. Duan, L. W. Burggraf, and L. Huang, Molecules **18**, 8591 (2013).

[8]E. D. Glendening, J. K. Badenhoop, A. E. Reed, J. E. Carpenter, J. A. Bohmann, C. M. Morales, and F. Weinhold, NBO 5.0, Theoretical Chemistry Institute, University of Wisconsin, Madison, WI, 2001.

[9]A. V. Marenich, S. V. Jerome, C. J. Cramer, and D. G. Truhlar, J. Chem. Theory Comput. **8**, 527 (2012).

[10]K. A. Wiberg, Tetrahedron **24**, 1083 (1966).

[11]C. Peng and H. B. Schlegel, Isr. J. Chem. **33**, 449 (1993).

[12]A. D. Becke, J. Chem. Phys. **98**, 5648 (1993).

[13]R. A. Kendall, T. H. Dunning, Jr., and R. J. Harrison, J. Chem. Phys. **96**, 6796 (1992).

[14]C. Adamo and V. Barone, J. Chem. Phys. **110**, 6158 (1999).

[15]A. D. Becke, Phys. Rev. A **38**, 3098 (1988).

[16]C. Lee, W. Yang, and R. G. Parr, Phys. Rev. B **37**, 785 (1988).

[17]J. Frisch, G. W. Trucks, H. B. Schlegel, G. E. Scuseria, M. A. Robb, J. R. Cheeseman, G. Scalmani, V. Barone, B. Mennucci, G. A. Petersson *et al.*, GAUSSIAN 09, Revision D.1, Gaussian, Inc., Wallingford, CT, 2009.

[18]S. I. Gorelsky, SWizard, University of Ottawa, Canada, 2013, available at http://www.sg-chem.net/.

[19]P. Delhaes, *Graphite and Precursors* (CRC Press, 2001), ISBN: 90-5699-228-7.

[20]J. C. Yang, W. G. Xu, and W. S. Xiao, J. Mol. Struct.: THEOCHEM **719**, 89–102 (2005); R. Fournier, S. B. Sinnott, and A. E. DePristo, J. Chem. Phys. **97**, 4149 (1992); K. Balasubramanian, Chem. Phys. Lett. **135**, 283 (1987).

[21]X. Duan, J. Wei, L. Burggraf, and D. Weeks, Comput. Mater. Sci. **47**, 630 (2010).

[22]*Handbook of Thin Films Materials, Nanomaterials and Magnetic Thin Films*, edited by H. S. Nalwa (Academic Press, 2002), Vol. 5.

[23]X. Zhang, Q. Zhou, Y. Huang, Z. Li, and Z. Zhang, Sensors **11**, 11510 (2011).

[24]B. Song, Y. Yong, J. Hou, and P. He, Eur. Phys. J. D **59**, 399 (2010).